ASYMPTOTIC ANALYSIS OF A MULTIPHASE DRYING MODEL MOTIVATED BY COFFEE BEAN ROASTING *

NABIL T. FADAI†, COLIN P. PLEASE†, AND ROBERT A. VAN GORDER†

Abstract. Recent modelling of coffee bean roasting suggests that in the early stages of roasting, within each coffee bean, there are two emergent regions: a dried outer region and a saturated interior region. The two regions are separated by a transition layer (or, drying front). In this paper, we consider the asymptotic analysis of a multiphase model of this roasting process which was recently put forth and studied numerically, in order to gain a better understanding of its salient features. The model consists of a PDE system governing the thermal, moisture, and gas pressure profiles throughout the interior of the bean. Obtaining asymptotic expansions for these quantities in relevant limits of the physical parameters, we are able to determine the qualitative behaviour of the outer and interior regions, as well as the dynamics of the drying front. Although a number of simplifications and scaling are used, we take care not to discard aspects of the model which are fundamental to the roasting process. Indeed, we find that for all of the asymptotic limits considered, our approximate solutions faithfully reproduce the qualitative features evident from numerical simulations of the full model. From these asymptotic results we have a better qualitative understanding of the drying front (which is hard to resolve precisely in numerical simulations), and hence of the various mechanisms at play as heating, evaporation, and pressure changes result in a roasted bean. This qualitative understanding of solutions to the multiphase model is essential if one is to create more involved models that incorporate chemical reactions and solid mechanics effects.

Key words. multiphase model, coffee bean roasting, Stefan problem, asymptotic analysis, drying front

AMS subject classifications. 80A22, 80M35, 74N20, 82C26

1. Introduction.

As one of the most valuable commodities in the world [1], the coffee industry relies on fundamental research to improve the techniques and processes relating to its products. In particular, in this paper, we will focus on the roasting process of coffee beans. Most of the literature concerning the roasting of coffee beans present experimental data (see e.g. [2, 3, 4]), and use regression analysis and simple empirical models to interpret the results. Recently, the literature has included a more in-depth discussion concerning the mathematical modelling of the roasting of coffee beans (see e.g. [5, 6]). While other aspects of coffee processing have been examined from a mathematical perspective (e.g. [7]), mathematical models to describe the roasting of coffee beans have, with the exception of a few studies, been largely unexplored.

In [5], a system of partial differential equations (PDEs) modelling the transport of moisture and heat throughout a coffee bean were derived and studied. This model uses the concept of "mass diffusivity" to describe the transport of moisture in the coffee bean that was originally derived in [8], which applies to lower-temperature evaporation. The ideas in [5] served as excellent motivation for the authors in [6] to derive a mathematical model from first principles using conservation equations. In [6], the concept of multiphase flow and water evaporation were included, and the resulting multiphase model (referred to as Model 2 in [6]) incorporated the production of carbon dioxide gas, latent heat due to evaporation within the coffee bean, and the changing porosity of the bean. The use of multiphase modelling was previously applied in a variety of food heating problems [9, 10, 11, 12, 13, 14] (of particular relevance was the bread baking model of Zhang et al. [15]), and is a natural framework to model the coffee bean roasting process. Some simplifications were made to this full model (in particular, neglecting carbon dioxide production) in order to allow some preliminary understanding of the model behaviour. By examining the numerical solution of this multiphase model, a "drying front" that propagates through to the center of the bean.

Mathematical models describing drying have been explored previously (see e.g. [16, 17, 18]), which relate the drying of wood, bricks, and other materials. However, in these models, the crucial parameter regime being explored is when water vapour produced from evaporation can easily permeate through the material and reach the external environment. Due to the rigid, impermeable cellulose structure within a coffee bean, the water vapour created in a coffee bean's biological cells cannot be easily released into the roasting environment. In consequence, the ratio between evaporation dynamics and vapour transport is very large, which motivates us to explore the leading-order dynamics of coffee bean roasting using asymptotic analysis. Hence, the model presented here should be appropriate to any drying problem where these physical

*This publication is based on work supported by the EPSRC center for Doctoral Training in Industrially Focused Mathematical Modelling (EP/L015803/1)

†Mathematical Institute, University of Oxford, Andrew Wiles Building, Radcliffe Observatory Quarter, Woodstock Road, Oxford, OX2 6GG, United Kingdom (Robert.VanGorder@maths.ox.ac.uk)

phenomena are relevant.

As we have seen previously in [6], numerical results suggest that there are three main regions within a coffee bean as it is roasted. The first main region (which we refer to as Region i) is where the vapour pressure of water aligns with the steam table pressure. The second main region (which we refer to as Region ii) is when the moisture content of the bean is negligible. Between these two regions, we expect a thin transition layer, or "drying front", in which the moisture content is rapidly evaporated away. Issues surrounding numerical resolution make it difficult to resolve the dynamics near the drying front. In light of these observations, we are motivated to extend the numerical results shown in [6] via asymptotic methods in order to understand the qualitative features of the multiphase model, and in particular, the interplay between the transition layer and the two larger regions.

In the present paper, we begin our discussion of the asymptotics of the full multiphase model in Sec. 2. Motivated by the numerical results seen in [6], we determine an approximate form of the drying front. We then obtain the leading-order asymptotics in Regions i and ii, as well as within the drying front. Despite several simplifications, we are able to obtain reasonable agreement between the asymptotic approximations and the numerical solution of the multiphase model described in [6], and are confident that the asymptotics capture the qualitative dynamics of the problem. In order to obtain more explicit results, and motivated by the fact that the coffee bean is at roasting temperature throughout most of the roasting process, in Sec. 3 we fix the temperature at the roasting temperature. Under this assumption, the vapour pressure and moisture content remain constant to leading order in Region i, while the the dynamics within Region ii reduce to a Stefan problem [19], to leading order. By considering the case of a large Stefan number limit, we determine a leading-order expression for the drying front for various geometries. As we will only focus on symmetric geometries (e.g. planar and spherical geometries), we can obtain explicit expressions for the drying front where there is only one spatial variable. This single spatial variable will be denoted as r in all geometries considered. We focus on the planar and spherical geometries in particular as it is reasonable to represent a coffee bean either as a sphere, or as a slab of porous material "curled up" into the shape of a bean. In [6] and in Secs. 2-3, the evaporation is modelled by Langmuir's evaporation equation [20], and this may not be the most accurate way to represent the evaporation of water in a coffee bean. Therefore, in Sec. 4, we consider a more general evaporation rate for the multiphase model. While the dynamics inside the drying front, where evaporation dominates water transport, will vary, we determine that the qualitative behaviour in Regions i and ii remains unchanged to this larger class of evaporation rates, suggesting that the explicit choice of evaporation equation is not pivotal to a qualitative understanding of coffee bean roasting. Finally, in Sec. 5, we provide a summary and discussion of the results.

2. Asymptotics of the Multiphase Model with Variable Temperature.

The full multiphase model that we will analyse is described by the PDEs in symmetric geometries (i.e. using a single spatial variable r)

$$\frac{\partial S}{\partial t} = -\frac{1}{\epsilon^2} I_v, \tag{1}$$

$$\frac{\partial}{\partial t}\left[\frac{(1+\mathscr{T})P(1-\sigma S)}{1+\mathscr{T}T}\right] = -\frac{1}{\delta}\frac{\partial S}{\partial t} + \nabla\cdot\left[\frac{(1+\mathscr{T})P\nabla P}{1+\mathscr{T}T}\right], \tag{2}$$

$$\frac{\partial T}{\partial t} + \mathcal{A}_1\frac{\partial}{\partial t}\left[S(1+\mathscr{T}T)\right] = \mathcal{A}_2\frac{\partial S}{\partial t} + \mathcal{A}_3\nabla\cdot\left[(1+\mathcal{A}_4 S)\nabla T\right], \tag{3}$$

with the symmetry conditions at the centre of the bean (i.e. $r = 0$)

$$\nabla T\cdot\mathbf{n} = 0, \quad \nabla P\cdot\mathbf{n} = 0, \tag{4}$$

the boundary conditions at the surface of the bean (i.e. $r = 1$)

$$\nabla T\cdot\mathbf{n} = \nu\left(\frac{1-\sigma S}{1-\sigma}\right)\left(\frac{1+\mathcal{A}_4}{1+\mathcal{A}_4 S}\right)(1-T), \tag{5}$$

$$P = \begin{cases} P_{ST}(T), & T < T_a, \\ P_a, & T \geq T_a, \end{cases} \tag{6}$$

and the initial conditions

$$S(r,0)=1,\quad T(r,0)=0,\quad P(r,0)=P_{ST}(0). \tag{7}$$

Here, the evaporation rate I_v and steam table pressure $P_{ST}(T)$ are given by

$$I_v = S(1-\sigma S)(P_{ST}-P)\sqrt{\frac{1+\mathscr{T}}{1+\mathscr{T}T}} \quad \text{and} \quad P_{ST}(T)=\exp\left(\frac{\beta(T-1)}{1+\mathscr{T}T}\right). \tag{8}$$

A complete derivation of this model from the "simplified" multiphase model presented in [6] can be found in Appendix A. Here, S is the saturation (the volume fraction of water divided by the total volume of water and gas), I_v is the evaporation rate of water, P is the partial pressure of water vapour, T is the normalized temperature, and p_{ST} is the steam table pressure. Our three PDEs describe conservation of mass in water and vapour, as well as conservation of energy. The only transport mechanism considered for water is via evaporation, whereas in the gas phase, water vapour is transported either via evaporation or via Darcy flow. Finally, we assume that heat is transported via conduction in all three phases within the bean, but via convection at the surface of the bean. A key feature of this model is ϵ, which can be interpreted as a rescaled ratio between Darcy-driven vapour transport and evaporation. One can interpret δ as a rescaled density ratio of water vapour to water, and σ represents the initial water-to-void volume ratio. The boundary condition (6) is slightly modified from that in [6] and is described in Appendix A. Here, P_a is the ambient vapour pressure in the roasting chamber. We will also make the assumption that the change in boundary conditions for P only occurs at one critical time, namely, t^*. We define t^* as when the time when the evaporation temperature T_a is achieved at the surface of the bean, i.e. as the solution to the equation

$$T(1,t^*)=T_a := P_{ST}^{-1}(P_a)\,. \tag{9}$$

This critical time will be used not only to signal the transition from one asymptotic region to another, but also to determine the form of the boundary conditions to be used.

We divide our system of PDEs into three regions in order to understand the approximate dynamics that occur in each region of the coffee bean. Using parameter values shown in [6], a typical value of $\epsilon \approx 1.54\times10^{-4}$ suggests that we should consider the limit of $\epsilon \to 0^+$. Therefore, we will assume that $\epsilon \ll 1$, δ is either $O(1)$ or $\ll 1$, depending on which region were are examining, and all other parameters are $O(1)$. In this limit, we can see from (1) that if time and space remain unscaled, $I_v = 0$ will be our leading-order equation, and from (8), this can occur in one of three ways. The first is if the vapour pressure is in equilibrium with its steam table pressure, i.e. $P = P_{ST}$. As the initial data is consistent with the vapour pressure in equilibrium with its steam table pressure, this will be the first case we will observe (which will be referred to as Region i). Secondly, $I_v = 0$ can be achieved by setting $S = 0$. This corresponds to where there is no more water to evaporate off, and will be denoted as Region ii. A final case where $I_v = 0$ is when $S = \sigma^{-1}$; however, this corresponds to when the coffee bean is completely saturated with water, which we will discard as an extraneous case.

We will also consider a narrow "drying front" that connects the two physically relevant asymptotic regions where $I_v = 0$ (Regions i and ii). This drying front, which is centred about $r = R(t)$, propagates from the surface of the bean towards the center of the bean and is where the moisture content S quickly goes from 1 to 0. In this drying front around $R(t)$, we find that the temperature is spatially uniform, but will vary as time progresses. The temperature profile within the drying front is denoted as $T^*(t)$. A schematic diagram of these three regions is shown in Figure 1, including the time t^* at which evaporation first occurs at the surface of the bean.

We will now discuss the leading-order asymptotics of the three main regions in the limit of $\epsilon \to 0^+$ and, where applicable, the additional limit of $\delta \to 0^+$. In Region i, where $P = P_{ST}$ at leading-order, our leading-order equations will reduce to a system of two PDEs for S and T. However, we will only be able to obtain analytic results if we further expand the leading-order solution in ϵ with an asymptotic series in δ. As we are only concerned with the leading-order asymptotic behaviour in Region i, we will not worry about the relative magnitude between ϵ and δ, where we might observe cross-terms at higher orders. With this additional simplification, we determine that S is constant at leading-order, and T can be described by the heat equation. We can then determine a leading-order approximation of t^*, which is the solution of a

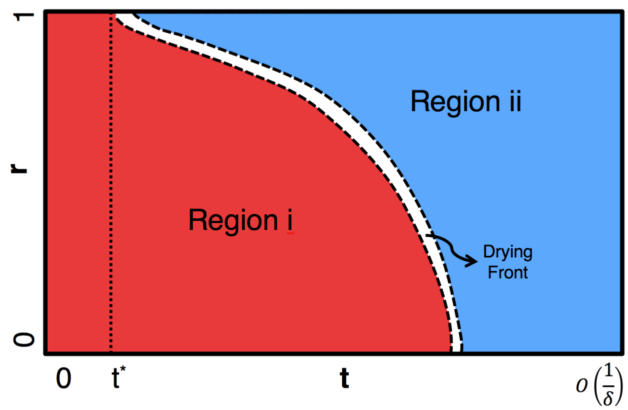

FIG. 1. *A summary of where the different regions are as the bean dries. Region i is when the vapour pressure is in equilibrium, Region ii is the dry region, and the dashed lines indicate the narrow transition layer between the regions, which begins at time t^*, defined in* (9).

transcendental equation. However, we note that for $t \geq t^*$, Region i is bounded in r between the drying front $R(t)$ and the centre of the bean, and we cannot find any analytic results via similarity solutions or separation of variables.

In order for Region ii to exist, we must have a transition layer in which S changes from 1 to 0. We expect this "drying front" to progress to the center of the bean. In this thin region, we will determine the leading-order ODE that governs the dynamics of S. In order to match with Region i, we also must have that T and P do not vary in space at leading-order; they will, however, vary in time. In consequence, our leading-order solution for T is denoted by $T^*(t)$, and for P to match with Region i, its leading-order solution is $P_{ST}(T^*(t))$. We will then show that the first order correction terms to T and P can be expressed in terms of the leading-order solution of S in the transition layer. While greater care needs to be taken when the transition layer is near the surface and centre of the bean, we will assume that the same dynamics in the rest of the transition layer apply at these endpoints. It is also important to note that we will assume that $\delta = O(1)$ in the transition layer.

Finally, we examine Region ii, where the evaporation has stopped due to lack of water. From our higher-order matching from exiting the transition layer, as well as the coupled PDE system for T and P, this gives us a Stefan problem in Region ii to not only determine T and P, but also $R(t)$ and $T^*(t)$. By assuming once again that $\delta \ll 1$, we obtain via a further asymptotic expansion the leading-order behaviour of T^*, R, P, and T in Cartesian and spherical geometries.

2.1. Asymptotics of Region i. In Region i, we have, from (1), $I_v = 0$ to leading order in the limit of $\epsilon \to 0^+$, implying that that $P = P_{ST}(T)$. Consider the asymptotic series valid as $\epsilon \to 0^+$,

$$S = S_0(r,t) + \epsilon S_1(r,t) + O(\epsilon^2), \quad T = T_0(r,t) + \epsilon T_1(r,t) + O(\epsilon^2), \quad P = P_{ST}(r,t) + \epsilon P_1(r,t) + O(\epsilon^2). \tag{10}$$

Substituting these asymptotic expansions into (2) and (3) gives us to lowest order

$$\frac{\partial S_0}{\partial t}\left(\frac{1}{\delta} - \sigma P_{ST}(T_0)\Lambda(T_0)\right) + (1-\sigma S_0)\frac{\partial}{\partial t}\left[P_{ST}(T_0)\Lambda(T_0)\right] = \nabla \cdot \left[P_{ST}(T_0)\Lambda(T_0)\nabla P_{ST}(T_0)\right], \tag{11}$$

$$\frac{\partial S_0}{\partial t}\left(\mathcal{A}_1(1+\mathscr{T}T_0) - \mathcal{A}_2\right) + \frac{\partial T_0}{\partial t}\left[1 + \mathcal{A}_1\mathscr{T}S_0\right] = \mathcal{A}_3\nabla \cdot \left[(1+\mathcal{A}_4 S_0)\nabla T_0\right], \tag{12}$$

where $\Lambda(T_0) = \frac{1}{1+\mathscr{T}T_0}$. As we cannot solve this system analytically, we now suppose that $\delta \ll 1$ and write an asymptotic series in powers of δ for S_0 and T_0 valid in the limit $\delta \to 0^+$ as

$$S_0 = \tilde{S}_0(r,t) + \delta\tilde{S}_1(r,t) + O(\delta^2), \quad T_0 = \tilde{T}_0(r,t) + \delta\tilde{T}_1(r,t) + O(\delta^2). \tag{13}$$

Substituting these asymptotic expansions into (11) gives us, to leading order, that $\frac{\partial \tilde{S}_0}{\partial t} = 0$. Therefore, the moisture content of the bean stays at its initial value, i.e. $\tilde{S}_0 = 1$. To lowest order, (12) then gives us

$$\frac{\partial \tilde{T}_0}{\partial t} = \mathcal{K}\nabla^2\tilde{T}_0, \quad \text{where} \quad \mathcal{K} = \frac{\mathcal{A}_3(1+\mathcal{A}_4)}{1+\mathcal{A}_1\mathscr{T}}. \tag{14}$$

Equation (14) has a time-dependent boundary condition, which depends on if evaporation has begun at the surface of the bean. This can be stated as

$$\nabla \cdot \tilde{T}_0\Big|_{r=1} = \nu \left(1 - \tilde{T}_0\big|_{r=1}\right), \quad t < t^*, \tag{15}$$

$$\tilde{T}_0\Big|_{r=R(t)} = T^*(t), \quad t \geq t^*. \tag{16}$$

Additionally, we will continue to impose the symmetry condition $\nabla\tilde{T}_0 \cdot \mathbf{n} = 0$ at $r = 0$, as well as the initial data $\tilde{T}_0(r, 0) = 0$. We are able to solve the PDE for $t < t^*$, and in particular, determine a leading-order approximation for t^*. By solving (14) in spherical co-ordinates, we obtain that

$$\tilde{T}_0(r, t) = 1 - \sum_{n=1}^{\infty} \frac{c_n}{r} \sin(\mu_n r) \exp(-\mu_n^2 \mathcal{K} t). \tag{17}$$

where the eigenvalues μ_n satisfy the transcendental equation $\mu_n \cot(\mu_n) = 1 - \nu$ and the constants c_n have the form

$$c_n = \begin{cases} \frac{2\nu \cos \mu_n}{\mu_n(\sin^2 \mu_n - \nu)}, & \nu \neq 1, \\ \frac{8(-1)^n}{\pi^2(1+2n)^2}, & \nu = 1. \end{cases} \tag{18}$$

To determine t^* in spherical co-ordinates, denoted as t^*_{Sph}, we impose, from (9), that $\tilde{T}_0(1, t^*_{\text{Sph}}) = T_a$. When $\nu \neq 1$, this is equivalent to writing

$$\sum_{n=1}^{\infty} \left(\frac{\cos^2 \mu_n}{\sin^2 \mu_n - \nu}\right) \exp(-\mu_n^2 \mathcal{K} t^*_{\text{Sph}}) = \frac{(1 - T_a)(1 - \nu)}{2\nu}, \tag{19}$$

or when $\nu = 1$,

$$\sum_{n=1}^{\infty} \frac{\exp\left(-\frac{\mathcal{K}\pi^2}{4}(1 + 2n)^2 t^*_{\text{Sph}}\right)}{(1 + 2n)^2} = \frac{\pi^2(1 - T_a)}{8}. \tag{20}$$

Using parameter values shown in [6], yielding $\mathcal{K} \approx 2.25, \nu \approx 0.585, T_a \approx 0.519$, this gives us that $t^*_{\text{Sph}} \approx 0.173$, or about 45.9 seconds in dimensional units.

Similarly, we can determine t^* in Cartesian co-ordinates, denoted as t^*_{Cart}, by determining that the solution of (14) in Cartesian co-ordinates, with a Neumann boundary condition at $r = 0$, is

$$\tilde{T}_0(r, t) = 1 - \sum_{n=1}^{\infty} d_n \cos(\lambda_n r) \exp(-\lambda_n^2 \mathcal{K} t), \tag{21}$$

where

$$\lambda_n \tan \lambda_n = \nu \quad \text{and} \quad d_n = \frac{2\nu \sin \lambda_n}{\lambda_n(\nu + \sin^2 \lambda_n)}. \tag{22}$$

This in turn allows us to determine t^*_{Cart} via the transcendental equation

$$\sum_{n=1}^{\infty} \frac{\sin^2 \lambda_n}{\nu + \sin^2 \lambda_n} \exp(-\lambda_n^2 \mathcal{K} t^*_{\text{Cart}}) = \frac{1 - T_a}{2}, \tag{23}$$

which, using parameter values stated above, gives us that $t^*_{\text{Cart}} \approx 0.494$, or about 131 seconds in dimensional units.

2.2. Asymptotics of the Transition Layer. In order to understand how S varies from 1 to 0, we must examine the transition layer in the $\epsilon \to 0^+$ limit, with all other parameters (including δ) being $O(1)$. We expect that this transition layer will happen when r is close to the "drying front" $R(t)$, so we introduce the scaling $r = R(t) + \epsilon\hat{r}$. Once again, we can expand P, T, and S as asymptotic series as $\epsilon \to 0^+$,

$$S = S_0(\hat{r},t) + \epsilon\hat{S}_1(\hat{r},t) + O(\epsilon^2), \quad P = P_0(\hat{r},t) + \epsilon P_1(\hat{r},t) + O(\epsilon^2), \quad T = T_0(\hat{r},t) + \epsilon T_1(\hat{r},t) + O(\epsilon^2). \tag{24}$$

We will first show that $T_0(\hat{r},t) \equiv T^*(t)$ and $P_0(\hat{r},t) \equiv P^*(t) := P_{ST}(T^*(t))$. Do this, we note that, in order to match our transition layer into Region i, we must have that

$$P_0\big|_{\hat{r}\to-\infty} \to P^*(t) \quad \text{and} \quad T_0\big|_{\hat{r}\to-\infty} \to T^*(t). \tag{25}$$

By substituting (24) into (2) and (3), we obtain at $O\left(\epsilon^{-2}\right)$

$$\frac{\partial}{\partial\hat{r}}\left[\frac{P_0\frac{\partial P_0}{\partial\hat{r}}}{1+\mathscr{T}T_0}\right] = 0, \qquad \frac{\partial}{\partial\hat{r}}\left[\frac{\partial T_0}{\partial\hat{r}}(1+\mathcal{A}_4S_0)\right] = 0. \tag{26}$$

We note that these equations hold in any geometry at leading order, provided that we are sufficiently far away from any geometry-induced singularities that could produce additional derivative terms at $O\left(\epsilon^{-2}\right)$, e.g. if $R(t) = O(\epsilon)$ in spherical co-ordinates. Integrating (26) and imposing (25) implies that $T_0(\hat{r},t) \equiv T^*(t)$ and $P_0(\hat{r},t) \equiv P^*(t)$. To determine the leading-order behaviour for S, we note that using (24) in (8) and expanding gives

$$\begin{aligned} P_{ST} &= P^*\left(1 + \epsilon\frac{\beta(1+\mathscr{T})}{(1+\mathscr{T}T^*)^2}T_1\right) + O\left(\epsilon^2\right), \\ I_v &= -\epsilon\left(P_1 - \frac{\beta(1+\mathscr{T})}{(1+\mathscr{T}T^*)^2}T_1P^*\right)S_0(1-\sigma S_0)\sqrt{\frac{1+\mathscr{T}}{1+\mathscr{T}T^*}} + O\left(\epsilon^2\right). \end{aligned} \tag{27}$$

Using these along with (25), we obtain, at $O(\epsilon^{-1})$, that (1)-(3) give

$$-R'(t)\frac{\partial S_0}{\partial\hat{r}} = \Psi(P_1,T_1)S_0(1-\sigma S_0), \tag{28}$$

$$\sigma P^*R'(t)\frac{\partial S_0}{\partial\hat{r}} = -\frac{1}{\delta}\Psi(P_1,T_1)S_0(1-\sigma S_0)\left(\frac{1+\mathscr{T}T^*}{1+\mathscr{T}}\right) + P^*\frac{\partial^2P_1}{\partial\hat{r}^2}, \tag{29}$$

$$-\mathcal{A}_1(1+\mathscr{T}T^*)R'(t)\frac{\partial S_0}{\partial\hat{r}} = \mathcal{A}_2\Psi(P_1,T_1)S_0(1-\sigma S_0) + \mathcal{A}_3\frac{\partial}{\partial\hat{r}}\left[(1+\mathcal{A}_4S_0)\frac{\partial T_1}{\partial\hat{r}}\right], \tag{30}$$

where

$$\Psi(P_1,T_1) := \sqrt{\frac{1+\mathscr{T}}{1+\mathscr{T}T^*}}\left(P_1 - \frac{\beta(1+\mathscr{T})}{(1+\mathscr{T}T^*)^2}T_1P^*\right). \tag{31}$$

Finally, the matching conditions with Regions i and ii are

$$S_0 \to 1, \quad P_1 \to 0, \quad \text{and} \quad T_1 \to 0 \quad \text{as} \quad \hat{r} \to -\infty, \tag{32}$$

$$S_0 \to 0 \quad \text{as} \quad \hat{r} \to +\infty, \tag{33}$$

$$\frac{\partial P_1}{\partial\hat{r}}\Big|_{\hat{r}\to+\infty} = \frac{\partial P}{\partial r}\Big|_{r\to R(t)}, \tag{34}$$

$$\frac{\partial T_1}{\partial\hat{r}}\Big|_{\hat{r}\to+\infty} = \frac{\partial T}{\partial r}\Big|_{r\to R(t)}. \tag{35}$$

In interpreting (32)-(35), we note that the limits where $r \to R(t)$ are matching conditions for Regions i and ii, whereas the limits where $\hat{r} \to \pm\infty$ refer to matching conditions for the transition layer.

We will now show that in the transition layer, the terms P_1 and T_1 can both be expressed in terms of S_0 alone. Firstly, by eliminating the terms with $\Psi(P_1,T_1)$ in (28) and (29), we obtain

$$P^*\frac{\partial^2P_1}{\partial\hat{r}^2} = \left[\sigma P^* - \frac{1}{\delta}\left(\frac{1+\mathscr{T}T^*}{1+\mathscr{T}}\right)\right]R'(t)\frac{\partial S_0}{\partial\hat{r}}. \tag{36}$$

Integrating this and imposing the matching conditions (32) yields

$$\frac{\partial P_1}{\partial \hat{r}} = \left[\frac{1}{\delta}\left(\frac{1+\mathscr{T}T^*}{(1+\mathscr{T})P^*}\right) - \sigma\right] R'(t)(1-S_0). \tag{37}$$

Similarly, eliminating terms with $\Psi(P_1, T_1)$ in (28) and (30) gives us

$$R'(t)\left[\mathcal{A}_2 - \mathcal{A}_1(1+\mathscr{T}T^*)\right]\frac{\partial S_0}{\partial \hat{r}} = \mathcal{A}_3 \frac{\partial}{\partial \hat{r}}\left[(1+\mathcal{A}_4 S_0)\frac{\partial T_1}{\partial \hat{r}}\right]. \tag{38}$$

Integrating and imposing the matching conditions (32) yields, after some rearranging,

$$\frac{\partial T_1}{\partial \hat{r}} = -\frac{1}{\mathcal{A}_3} R'(t)\left[\mathcal{A}_2 - \mathcal{A}_1(1+\mathscr{T}T^*)\right]\left(\frac{1-S_0}{1+\mathcal{A}_4 S_0}\right). \tag{39}$$

Finally, by rearranging (28) to isolate S_0, we obtain

$$\frac{\frac{\partial S_0}{\partial \hat{r}}}{S_0(1-\sigma S_0)} = -\frac{\Psi(P_1, T_1)}{R'(t)}. \tag{40}$$

In order to write a single ODE for S_0, we differentiate (40) with respect to $\hat{r}$, as well as substitute in (37) and (39), to give us

$$\frac{\partial^2 S_0}{\partial \hat{r}^2} - \left(\frac{\partial S_0}{\partial \hat{r}}\right)^2 \frac{1-2\sigma S_0}{S_0(1-\sigma S_0)} + S_0(1-\sigma S_0)(1-S_0)\Upsilon(S_0) = 0, \tag{41}$$

where we define

$$\Upsilon(S_0) := \sqrt{\frac{1+\mathscr{T}}{1+\mathscr{T}T^*}}\left[\frac{1}{\delta}\left(\frac{1+\mathscr{T}T^*}{(1+\mathscr{T})P^*}\right) - \sigma - \left(\frac{\beta(1+\mathscr{T})P^*}{\mathcal{A}_3(1+\mathscr{T}T^*)^2}\right)\left(\frac{\mathcal{A}_2 - \mathcal{A}_1(1+\mathscr{T}T^*)}{1+\mathcal{A}_4 S_0}\right)\right]. \tag{42}$$

We note that, aside from the denominator $1+\mathcal{A}_4 S_0$, the components of the function $\Upsilon(S_0)$ are independent in $\hat{r}$. Let us assume that $S_0(\hat{r})$ is strictly monotone in $\hat{r}$. By taking $f(\hat{r}) = S_0(\hat{r})$ and $g(\hat{r}) = \frac{\partial S_0}{\partial \hat{r}}$, we can transform (41) into the system of first-order ODEs

$$\begin{cases} \frac{\partial f}{\partial \hat{r}} = g, \\ \frac{\partial g}{\partial \hat{r}} = g^2 \frac{1-2\sigma f}{f(1-\sigma f)} - f(1-\sigma f)(1-f)\Upsilon(f), \end{cases} \tag{43}$$

and dividing the second equation of (43) by the first equation gives us

$$\frac{dg}{df} = g\frac{1-2\sigma f}{f(1-\sigma f)} - \frac{f(1-\sigma f)(1-f)\Upsilon(f)}{g}. \tag{44}$$

By monotonicity of $S_0(\hat{r})$, the function $\frac{dg}{df}$ is well-defined. We identify equation (44) as a Bernoulli-like ODE; letting $w = g^2$, (44) becomes

$$\frac{dw}{df} = 2w\frac{1-2\sigma f}{f(1-\sigma f)} - 2f(1-\sigma f)(1-f)\Upsilon(f). \tag{45}$$

Our ODE system has now become a linear first-order ODE for $w(f)$. Multiplying both sides of (45) by the integrating factor $f^{-2}(1-\sigma f)^{-2}$ and imposing the matching conditions (33) and (32) gives us

$$g(f) = -f(1-\sigma f)\sqrt{2\int_f^1 \frac{(1-\chi)\Upsilon(\chi)}{\chi(1-\sigma\chi)}d\chi}\,. \tag{46}$$

Here, we pick $g(f) = -\sqrt{w(f)}$ to agree with f being a strictly monotone decreasing function (so that S_0 transitions from 1 to 0). Returning to our original variables gives us the first-order non-linear autonomous ODE for $S_0(\hat{r})$:

$$\frac{\partial S_0}{\partial \hat{r}} = -S_0(1-\sigma S_0)\sqrt{2\int_{S_0}^1 \frac{(1-\chi)\Upsilon(\chi)}{\chi(1-\sigma\chi)}d\chi}\,. \tag{47}$$

Hence, we conclude that P and T do not drastically change within the transition layer. Additionally, the $O(\epsilon)$ perturbations P_1 and T_1 can be related to S_0, which is the solution of a first-order ODE in $\hat{r}$.

2.3. Asymptotics of Region ii. While the leading-order dynamics of S, T, and P have been determined in the transition layer, we still do not have an explicit form for $R(t)$ and $T^*(t)$. To find these, we now examine Region ii, where zero water is present. From (1), we have that $S = 0$ at $O(\epsilon^{-2})$. However, this in turn causes a cascading effect in the asymptotic expansion in ϵ of (1), and we conclude that $S = o(\epsilon^n)$ for all natural numbers n. Assuming the asymptotic series as $\epsilon \to 0^+$

$$T = T_0(r,t) + \epsilon T_1(r,t) + O(\epsilon^2), \quad P = P_0(r,t) + \epsilon P_1(r,t) + O(\epsilon^2), \tag{48}$$

and incorporating these substitutions into (2) and (3), we obtain

$$\frac{\partial}{\partial t}\left[\frac{P_0}{1+\mathscr{T}T_0}\right] = \nabla \cdot \left[\frac{P_0 \nabla P_0}{1+\mathscr{T}T_0}\right], \tag{49}$$

$$\frac{\partial T_0}{\partial t} = \mathcal{A}_3 \nabla^2 T_0. \tag{50}$$

For our boundary conditions in Region ii, we have the matching conditions, and these imply that (33)-(35)

$$T_0\big|_{r\to R(t)} \to T^*(t), \quad P_0\big|_{r\to R(t)} \to P^*(t), \tag{51}$$

$$\frac{\partial P_0}{\partial r}\bigg|_{r\to R(t)} = \frac{\partial P_1}{\partial \hat{r}}\bigg|_{\hat{r}\to+\infty} \to \left[\frac{1}{\delta}\left(\frac{1+\mathscr{T}T^*}{(1+\mathscr{T})P^*}\right) - \sigma\right] R'(t), \tag{52}$$

$$\frac{\partial T_0}{\partial r}\bigg|_{r\to R(t)} = \frac{\partial T_1}{\partial \hat{r}}\bigg|_{\hat{r}\to+\infty} \to -\frac{1}{\mathcal{A}_3}\left[\mathcal{A}_2 - \mathcal{A}_1(1+\mathscr{T}T^*)\right] R'(t). \tag{53}$$

In interpreting (52) and (53), we note that the limits where $r \to R(t)$ are for Region ii asymptotic expansions, whereas the limits where $\hat{r} \to +\infty$ refer to the transition layer asymptotic expansions.

We must also give an initial condition for $R(t)$, i.e. where the drying front begins. As the drying front starts from the surface of the bean and at the threshold temperature for evaporation, our initial conditions can be described as $R(t^*) = 1$, $T^*(t^*) = T_a$. Finally, our solutions must also continue to agree with the external boundary conditions of the system, namely,

$$\frac{\partial T_0}{\partial r}\bigg|_{r=1} = \nu\left(\frac{1+\mathcal{A}_4}{1-\sigma}\right)\left[1 - T_0\big|_{r=1}\right] \quad \text{and} \quad P_0\big|_{r=1} = P_a. \tag{54}$$

Therefore, our leading-order problem exhibits a coupled system of two Stefan-like problems. Motivated by the large Stefan-number approximation, we again assume that $\delta \ll 1$. By rescaling time with $\tau = \delta(t - t^*)$, we can examine the asymptotic series

$$T_0 = \tilde{T}_0(r,\tau) + \delta \tilde{T}_1(r,\tau) + O(\delta^2), \quad P_0 = \tilde{P}_0(r,\tau) + \delta \tilde{P}_1(r,\tau) + O(\delta^2) \tag{55}$$

as $\delta \to 0^+$. In consequence, our leading-order Region ii problem (49)-(54) becomes

$$\nabla^2 \tilde{T}_0 = 0, \tag{56}$$

$$\nabla \cdot \left(\frac{P_0 \nabla \tilde{P}_0}{1+\mathscr{T}\tilde{T}_0}\right) = 0, \tag{57}$$

$$\tilde{T}_0\big|_{r\to R(\tau)} \to T^*(\tau), \tag{58}$$

$$\tilde{P}_0\big|_{r\to R(\tau)} \to P^*(\tau), \tag{59}$$

$$\frac{\partial \tilde{P}_0}{\partial r}\bigg|_{r\to R(\tau)} \to \left(\frac{1+\mathscr{T}T^*}{(1+\mathscr{T})P^*}\right) R'(\tau), \tag{60}$$

$$\frac{\partial \tilde{T}_0}{\partial r}\bigg|_{r\to R(\tau)} \to 0, \tag{61}$$

$$\frac{\partial \tilde{T}_0}{\partial r}\bigg|_{r=1} = \nu\left(\frac{1+\mathcal{A}_4}{1-\sigma}\right)\left[1 - \tilde{T}_0\big|_{r=1}\right], \tag{62}$$

$$\tilde{P}_0\big|_{r=1} = P_a, \tag{63}$$

$$R(0) = 1, \tag{64}$$

$$T^*(0) = T_a. \tag{65}$$

By solving (56) with boundary conditions (58) and (61), this implies that $\tilde{T}_0 \equiv T^*(\tau)$. However, by applying (62) to this solution, this forces $T^*(\tau) \equiv 1$. In consequence, this reduces our coupled Stefan problem into a Stefan problem for pressure alone, i.e.

$$\nabla \cdot \left(\tilde{P}_0 \nabla \tilde{P}_0 \right) = 0, \tag{66}$$

$$\tilde{P}_0 \big|_{r \to R(\tau)} \to 1, \tag{67}$$

$$\tilde{P}_0 \big|_{r=1} = P_a, \tag{68}$$

$$\frac{\partial \tilde{P}_0}{\partial r}\bigg|_{r \to R(\tau)} \to R'(\tau), \tag{69}$$

$$R(0) = 1. \tag{70}$$

However, this solution cannot satisfy the initial condition (65) for $T^*(t)$. For this to be resolved, we would have to consider the full problem in t rather than τ. As we have a Robin boundary condition in T on the surface of the bean, a similarity solution not possible in any geometry, and therefore, an analytic solution for (49)-(54) is not readily available.

2.3.1. Determining $R(t)$ in Cartesian Co-ordinates with $T^* \equiv 1$. In the limiting case where $\delta \ll 1$, i.e. $T^* \equiv 1$, we can solve (66) with boundary conditions (67) and (68), provided that we neglect any short-time discrepancies between the initial condition $T^*(0) = T_a$ and $T^* \equiv 1$. Solving this PDE system gives us

$$\tilde{P}_0(r, \tau) = \sqrt{1 - (1 - P_a^2) \left(\frac{r - R(\tau)}{1 - R(\tau)} \right)}. \tag{71}$$

Now, our Stefan condition (69) gives us the ODE

$$\frac{dR}{d\tau} = -\frac{1 - P_a^2}{2(1 - R)}. \tag{72}$$

Based on the initial condition from (70), our drying front in Cartesian co-ordinates based on leading-order asymptotics, $R_{\text{Cart}}(\tau)$, is

$$R_{\text{Cart}}(\tau) = 1 - \sqrt{(1 - P_a^2)\tau}. \tag{73}$$

By returning to the original timescale of Region ii, we determine that $\tilde{P}_0$ can be fully expressed in Cartesian co-ordinates as

$$\tilde{P}_0^{\text{Cart}}(r, t) = \sqrt{P_a^2 + (1 - r)\sqrt{\frac{1 - P_a^2}{\delta \left(t - t^*_{\text{Cart}} \right)}}}. \tag{74}$$

Finally, we determine from (73) that the time to completely dry a bean based on leading-order asymptotics is

$$t_{\text{Cart}}^{\text{dry}} = t^*_{\text{Cart}} + \frac{1}{\delta (1 - P_a^2)}. \tag{75}$$

Using parameter values shown in [6], as well as typical values $P_a = 0.0879$, $\delta = 0.1011$, $\sigma = 0.0842$, and $t^*_{\text{Cart}} \approx 0.494$, we compute that $t_{\text{Cart}}^{\text{dry}} \approx 10.46$, or about 2768 seconds in dimensional units.

2.3.2. Determining $R(t)$ in Spherical Co-ordinates with $T^* \equiv 1$. In the limiting case where $\delta \ll 1$, i.e. $T^* \equiv 1$, we have that in spherical co-ordinates, by solving (66) with boundary conditions (67) and (68), that

$$\tilde{P}_0(r, \tau) = \sqrt{1 - \left(\frac{1 - P_a^2}{r} \right) \left(\frac{r - R(\tau)}{1 - R(\tau)} \right)}, \tag{76}$$

and our Stefan condition (69) gives us the ODE

$$\frac{dR}{d\tau} = -\frac{1-P_a^2}{2R(1-R)}. \tag{77}$$

We use our initial condition (70) to give us, in implicit form, that the inverse function of the drying front in spherical co-ordinates, $\tau_{\mathrm{Sph}}(R)$, satisfies the equation

$$\tau_{\mathrm{Sph}}(R) = \frac{1-R^2(3-2R)}{3(1-P_a^2)}. \tag{78}$$

We can invert (78) and solve $R_{\mathrm{Sph}}(\tau)$ in the correct domain and range and obtain

$$R_{\mathrm{Sph}}(\tau) = \frac{1}{2}\left(1 - \frac{\exp\left(\frac{2\pi i}{3}\right)}{\Xi\left(3(1-P_a^2)\tau\right)} - \exp\left(\frac{-2\pi i}{3}\right)\Xi\left(3(1-P_a^2)\tau\right)\right), \tag{79}$$

where

$$\Xi(\chi) = \sqrt[3]{2\sqrt{\chi(\chi-1)} - 2\chi + 1} \tag{80}$$

and $\Xi(\chi)$ uses the principal branch of the cube root. Now that we have determined $R(\tau)$ in spherical co-ordinates, we can return to our original timescale of the problem and obtain that our leading-order asymptotic approximation for P is

$$\tilde{P}_0^{\mathrm{Sph}}(r,t) = \sqrt{1 - \left(\frac{1-P_a^2}{r}\right)\left(1 - \frac{2(1-r)}{1 + \frac{\exp\left(\frac{2\pi i}{3}\right)}{\Xi\left(3\delta(1-P_a^2)(t-t^*_{\mathrm{Sph}})\right)} + \exp\left(\frac{-2\pi i}{3}\right)\Xi\left(3\delta(1-P_a^2)(t-t^*_{\mathrm{Sph}})\right)}\right)}. \tag{81}$$

To determine the time where the bean becomes fully dry, we substitute $R = 0$ into (78) to obtain, in our original timescale, that

$$t^{\mathrm{dry}}_{\mathrm{Sph}} = t^*_{\mathrm{Sph}} + \frac{1}{3\delta(1-P_a^2)}. \tag{82}$$

Therefore, to leading order, the time for a spherical coffee bean to dry out completely is $t^{\mathrm{dry}}_{\mathrm{Sph}} \approx 3.495$, or about 925 seconds in dimensional units. Figure 2(a) shows a comparison between the Cartesian and spherical asymptotic approximations of $R(t)$.

2.4. Comparison of Asymptotic Approximations with Numerical Results. We now compare these asymptotic approximations with the numerical solution of the PDE system (1)-(3). In particular, the main result that we wish to consider from the asymptotics is the approximate form of the drying front $R(t)$. As we can see in Figure 2(b), the general shape of the dimensional drying front $R(t)$ agrees reasonably well with the dimensional drying front seen in the numerical solution, especially as $R(t) \to 0$. However, we also see that the drying time in the numerical solution is larger than the predicted $t^{\mathrm{dry}}_{\mathrm{Sph}}$ from asymptotic results. This is to be expected, as the asymptotic results used were for when the Stefan number $\frac{1}{\delta} \to +\infty$. Therefore, for a smaller (but still large) Stefan number, we expect the drying time to be longer. Additionally, these approximations for the drying front $R(t)$ only hold for the critical assumption $T^* \equiv 1$. Because $T^*(t)$ will be less than unity, this will cause the drying front to be slower than the asymptotic approximation, which can explain why the numerical solution takes longer to dry out the entire bean.

3. Asymptotics of the Multiphase Model with Constant Temperature. In Section 2, we have given an analysis of the leading-order equations governing Region i, Region ii, and the transition layer. However, many of the leading-order equations cannot be solved unless a second asymptotic limit (in δ) is taken. Note that in this limit, the temperature within Region ii is, at leading-order, at roasting temperature. As the thermal timescale of the multiphase model is much smaller than the vapour diffusive timescale,

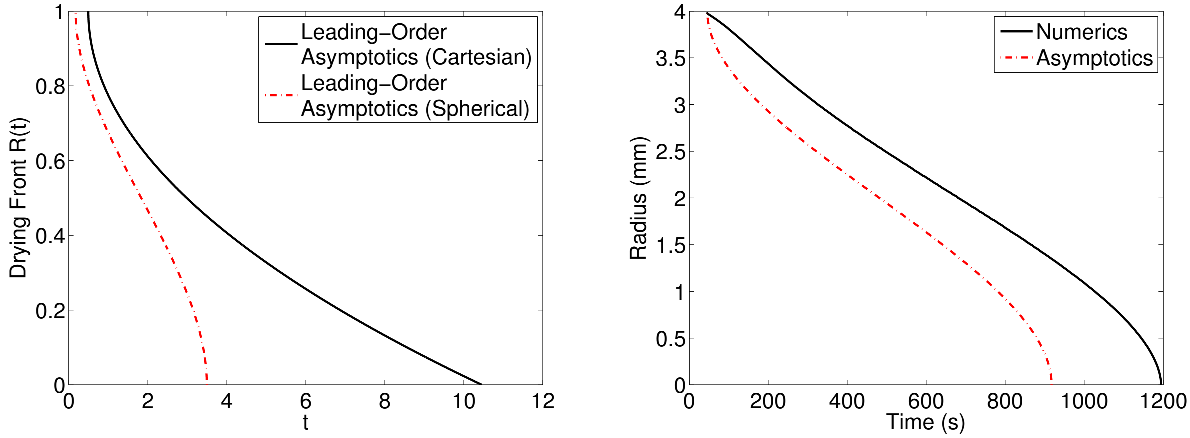

(a) (b)

FIG. 2. *(a) Comparison of the drying fronts $R_{Cart}(t)$ and $R_{Sph}(t)$. (b) Comparison of the dimensional drying front $R_{Sph}(t)$, shown in dash-dot red, against the numerical solution of the (dimensional) "simplified" multiphase model from [6] in spherical co-ordinates, shown in black.*

it seems reasonable to examine a simplified model where the coffee bean is held at roasting temperature throughout.

In this section, we will now impose that $T \equiv 1$ throughout the bean, which reduces the multiphase model to a PDE system in two variables. In consequence, this means that evaporation starts at the beginning of roasting rather than after a threshold amount of time (i.e. $t^* = 0$) and our system of PDEs (1)-(2) become

$$\frac{\partial S}{\partial t} = -\frac{1}{\epsilon^2}(1-P)S(1-\sigma S), \tag{83}$$

$$\frac{\partial}{\partial t}\left[(1-\sigma S)P\right] = \frac{1}{\delta\epsilon^2}(1-P)S(1-\sigma S) + \nabla\cdot(P\nabla P), \tag{84}$$

with boundary conditions

$$P\Big|_{r=1} = P_a, \qquad \frac{\partial P}{\partial r}\Big|_{r=0} = 0, \tag{85}$$

and initial conditions

$$S(r,0) = 1, \quad P(r,0) = 1. \tag{86}$$

Formally, we will consider the asymptotics of this system in the limit as $\epsilon \to 0^+$; δ will either be $\ll 1$ or $O(1)$, and all other parameters are assumed to be $O(1)$.

3.1. Asymptotics in Region i. In Region i, we have that $P = 1$ to leading order. This automatically satisfies the internal Neuman boundary condition $P_r\big|_{r=0} = 0$. Therefore, by substituting (83) into (84), with $P \sim 1$, we have that, to leading order,

$$\frac{\partial}{\partial t}\left[(1-\sigma S)\right] = -\frac{1}{\delta}\frac{\partial S}{\partial t}. \tag{87}$$

For this to happen requires that $\frac{\partial S}{\partial t} = 0$. Thus, S is held at its initial value, i.e. $S \equiv 1$, and P, S are constant to leading order in Region i. It is important to note that, since we assume that Region i is never in contact with the surface of the bean, the boundary condition at $r = 1$ does not apply.

3.2. Asymptotics of the Transition Layer. As is done in Section 2, we introduce the scaling $r = R(t) + \epsilon\hat{r}$ to examine the behaviour as S transitions from 1 to 0. Again, we can expand P and S as asymptotic series as $\epsilon \to 0$:

$$S = S_0(\hat{r},t) + \epsilon S_1(\hat{r},t) + O(\epsilon^2), \quad P = 1 + \epsilon P_1(\hat{r},t) + O(\epsilon^2). \tag{88}$$

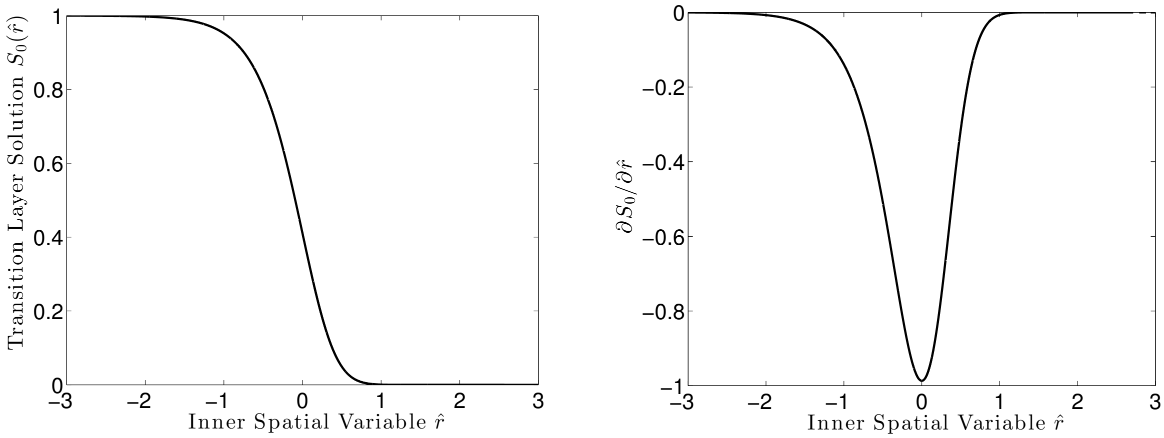

FIG. 3. *Numerical solution of the ODE (90). The left panel shows the solution $S_0(\hat{r})$, and the right panel shows its spatial derivative $\frac{\partial S_0}{\partial \hat{r}}$. For uniqueness, we pick a constant of integration so that $S_0(\hat{r})$ has an inflection point at $r = 0$.*

Noting that temperature is now constant (implying that $T_1 \equiv 0$ and $T^* \equiv 1$), our equation to $\Upsilon(S_0)$ shown in (42) reduces to $\Upsilon(S_0) \equiv \frac{1}{\delta} - \sigma$. From (37), this gives us

$$\frac{\partial P_1}{\partial \hat{r}} = \left(\frac{1}{\delta} - \sigma\right) R'(t)(1 - S_0), \tag{89}$$

and from (47), gives us the first-order non-linear autonomous ODE:

$$\frac{\partial S_0}{\partial \hat{r}} = -S_0(1 - \sigma S_0)\sqrt{2\left(\frac{1}{\delta} - \sigma\right)\left[\frac{1-\sigma}{\sigma}\log\left(\frac{1-\sigma}{1-\sigma S_0}\right) + \log\left(\frac{1}{S_0}\right)\right]}. \tag{90}$$

It is important to note a few key points about the ODE (90). Firstly, it is not explicitly solvable. Secondly, due to translational invariance, we require an additional constraint for uniqueness. This can be achieved by assuming the unique inflection point of S_0 occurs at $r = 0$. With this additional constraint, we numerically solve (90) and plot the results in Figure 3.

As we cannot obtain a closed-form solution to (90), we consider the asymptotic behaviour as $S_0(\hat{r})$ approaches either endpoint of the transition layer, i.e. as $\hat{r} \to \pm\infty$. While what is done here is not a formal asymptotic analysis, we can still use the results to find an approximation valid for all $\hat{r}$. To do this, we introduce the one-to-one transformation

$$\Phi(S_0) = \log\left(\frac{S_0}{1 - \sigma S_0}\right) \iff S_0(\Phi) = \frac{1}{\sigma + \exp(-\Phi)}, \tag{91}$$

which allows us to transform (90) into

$$\frac{\partial \Phi}{\partial \hat{r}} = -\sqrt{2\left(\frac{1}{\delta\sigma} - 1\right)\left(\log\left[(1-\sigma)^{1-\sigma}(\sigma\exp(\Phi) + 1)\right] - \sigma\Phi\right)}. \tag{92}$$

This transform from S_0 to Φ will allow us to compute a more accurate approximation as $\hat{r} \pm \infty$. We first examine the case when $\Phi \to -\infty$, which corresponds to the asymptotic behaviour of $S_0 \to 0^+$, and yields

$$\frac{\partial \Phi}{\partial \hat{r}} \sim -\sqrt{2\left(\frac{1}{\delta\sigma} - 1\right)\left((1-\sigma)\log(1-\sigma) - \sigma\Phi\right)} \quad \text{as} \quad \Phi \to -\infty. \tag{93}$$

By separating variables and integrating, we obtain that as $\hat{r} \to +\infty$,

$$\Phi(\hat{r}) \sim \left(\frac{1-\sigma}{\sigma}\right)\log(1-\sigma) - \frac{1}{2}\left(\frac{1}{\delta} - \sigma\right)(\hat{r} - C_1)^2, \tag{94}$$

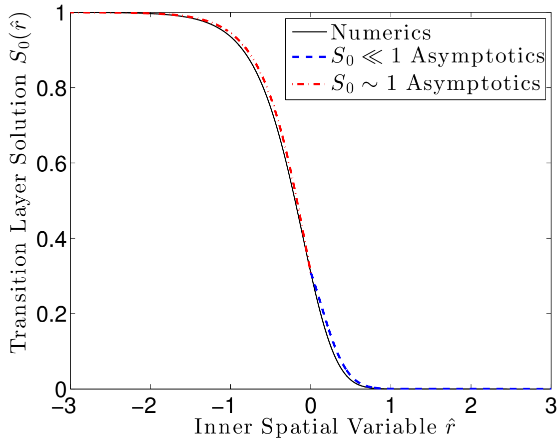

FIG. 4. *Comparison of the numerical solution $S_0(\hat{r})^{Num}$ with the approximate solutions for $S_0 \ll 1$, shown in (95), and for $S_0 \sim 1$, shown in (98). Constants in the approximate solutions are chosen so that continuity at the origin is held, as well as that the absolute error between the numerical solution and the approximate solutions is minimised.*

where C_1 is a constant of integration. Finally, we can use (91) which tells us that

$$S_0(\hat{r}) \sim \frac{1}{\sigma + (1-\sigma)^{-\frac{1-\sigma}{\sigma}} \exp\left(\frac{1-\delta\sigma}{2\delta}(\hat{r} - C_1)^2\right)} \quad \text{as } \hat{r} \to +\infty. \tag{95}$$

We note that this asymptotic approximation is only valid for when $\Phi \le \left(\frac{1-\sigma}{\sigma}\right) \log(1-\sigma)$, which is equivalent to stating that $\hat{r} \ge C_1$.

To construct an asymptotic approximation for (90) when $S_0 \sim 1$, i.e. when $\Phi \sim \log\left(\frac{1}{1-\sigma}\right)$, we note that

$$\frac{\partial \Phi}{\partial \hat{r}} \sim (\log(1-\sigma) + \Phi) \sqrt{\left(\frac{1}{\delta} - \sigma\right)(1-\sigma)}. \tag{96}$$

By separating variables and integrating, we see that

$$\Phi \sim -\log(1-\sigma) - C_2 \exp\left(\hat{r}\sqrt{\left(\frac{1}{\delta} - \sigma\right)(1-\sigma)}\right) \quad \text{as} \quad \hat{r} \to -\infty, \tag{97}$$

where C_2 is a constant of integration. Transforming back to S_0 using (91), this tells us that

$$S_0(\hat{r}) \sim \frac{1}{\sigma + (1-\sigma)\exp\left(C_2 \exp\left(\hat{r}\sqrt{\left(\frac{1}{\delta} - \sigma\right)(1-\sigma)}\right)\right)} \quad \text{as} \quad \hat{r} \to -\infty. \tag{98}$$

As this asymptotic expansion only has a singularity when $\Phi = -\log(1-\sigma)$, i.e. when $S_0 = 1$, this asymptotic approximation to the solution is valid for all $\hat{r}$.

Finally, in order to compare these asymptotic approximations to the numerical results shown in Figure 3, we wish to "patch" these two approximations together in a way that minimises the absolute error between the approximations and the numerical solution while still being valid for all $\hat{r}$. We can solve this minimisation problem numerically and obtain that, using parameter values shown in [6] as well as the typical values $\delta = 0.102$ and $\sigma = 0.0842$, the smallest maximum absolute error of ≈ 0.03092 is achieved when $C_1 \approx -0.1973$, and $C_2 \approx 1.235$. Additionally, in order for the asymptotic approximations to agree with the numerical solution $S_0(\hat{r})^{\text{Num}}$ at the origin, this implies that $S_0(0)^{\text{Num}} \approx 0.3092$. A comparison between the two asymptotic approximations and the numerical solution is shown in Figure 4, which shows good agreement for all $\hat{r}$.

3.3. Asymptotics in Region ii. In Region ii, we have, from (83), that $S = 0$ at $O(\epsilon^{-2})$, which again causes a cascading effect in the asymptotic expansion of (83). Therefore, we conclude that $S = o(\epsilon^n)$ for all natural numbers n. Additionally, by substituting the asymptotic series $P \sim P_0(r,t) + \epsilon P_1(r,t) + O(\epsilon^2)$, (84) becomes, at leading order,

$$\frac{\partial P_0}{\partial t} = \nabla \cdot (P_0 \nabla P_0) \,. \tag{99}$$

From (89), as well as noting that our evaporation start time $t^* = 0$ in this section, our boundary and initial conditions become

$$P_0\Big|_{r=1} = P_a, \qquad P_0\Big|_{r\to R(t)} \to 1, \qquad \frac{\partial P_0}{\partial r}\Big|_{r\to R(t)} \to \left(\frac{1}{\delta} - \sigma\right) R'(t), \qquad R(0) = 1. \tag{100}$$

One could interpret the PDE system (99)-(100) as a Stefan problem, with $\frac{1}{\delta} - \sigma$ acting as the Stefan constant. This problem has a similarity solution in Cartesian co-ordinates, as will be shown in Section 3.3.1, although it cannot be explicitly solved. However, we can also examine the physically relevant large Stefan-number limit by letting $\delta \to 0^+$, as was done in Section 2.3. By rescaling time with $\tau = \delta t$ and considering the asymptotic series $P_0 \sim \tilde{P}_0(r,\tau) + \delta \tilde{P}_1(r,\tau) + O(\delta^2)$, (99)-(100) become

$$\nabla \cdot \left(\tilde{P}_0 \nabla \tilde{P}_0\right) = 0, \quad \tilde{P}_0\Big|_{r=1} = P_a, \quad \tilde{P}_0\Big|_{r\to R(\tau)} \to 1, \quad \frac{\partial \tilde{P}_0}{\partial r}\Big|_{r\to R(\tau)} \to R'(t), \quad R(0) = 1. \tag{101}$$

Solving (101) like in Section 2, we determine that in Cartesian co-ordinates,

$$\tilde{P}_0(r,t) = \sqrt{P_a^2 + (1-r)\sqrt{\frac{1-P_a^2}{\delta t}}}, \quad R(t) = 1 - \sqrt{(1-P_a^2)\delta t}, \tag{102}$$

and in spherical co-ordinates,

$$\begin{aligned} \tilde{P}_0(r,t) &= \sqrt{1 - \left(\frac{1-P_a^2}{r}\right)\left[1 - \frac{2(1-r)}{1 + \frac{\exp\left(\frac{2\pi i}{3}\right)}{\Xi(3(1-P_a^2)\delta t)} + \frac{\Xi(3(1-P_a^2)\delta t)}{\exp\left(\frac{2\pi i}{3}\right)}}\right]}, \\ R(t) &= \frac{1}{2}\left(1 - \frac{\exp\left(\frac{2\pi i}{3}\right)}{\Xi\left(3(1-P_a^2)\delta t\right)} - \frac{\Xi\left(3(1-P_a^2)\delta t\right)}{\exp\left(\frac{2\pi i}{3}\right)}\right), \end{aligned} \tag{103}$$

where $\Xi(\chi) = \sqrt[3]{2\sqrt{\chi(\chi-1)} - 2\chi + 1}$.

3.3.1. Determining $R(t)$ in Cartesian Co-ordinates using Similarity Solutions. One might consider using a similarity solution to solve the system (99)-(100) without the assumption that $\delta \ll 1$. To do this, we let $P_0 = h(\eta)$, where $\eta = \frac{1-r}{\sqrt{t}}$. Substituting this transformation into (99) gives us, using Cartesian co-ordinates,

$$(h(\eta)h'(\eta))' + \frac{\eta}{2}h'(\eta) = 0, \tag{104}$$

and (100) becomes

$$h(0) = P_a, \qquad h(\lambda) = 1, \qquad h'(\lambda) = \frac{\lambda\,(1-\delta\sigma)}{2\delta}. \tag{105}$$

Here, $\eta = \lambda$ corresponds to the moving boundary $R(t)$. Thus, our drying front based on the Cartesian similarity solution, defined as $R_{\mathrm{SS}}(t)$, is therefore $1 - \lambda\sqrt{t}$. We note that our choice of η allows us to automatically satisfy the initial condition $R(0) = 1$. Thus, we can determine from this equation when the bean will be completely dry, i.e. when $R_{\mathrm{SS}}(t) = 0$. This gives us $t_{SS}^{\mathrm{dry}} = \frac{1}{\lambda^2}$. As (104) is not explicitly solvable, it is necessary to numerically solve this boundary value problem in order to determine λ. Using the shooting method, with the typical values $P_a = 0.0879$, $\delta = 0.1011$, and $\sigma = 0.0842$, we find that $\lambda \approx 0.3152$, implying that $t_{SS}^{\mathrm{dry}} \approx 10.06$, or about 2664 seconds in dimensional units. With less than a 1% relative error to t_{SS}^{dry}, we conclude that $t_{\mathrm{Cart}}^{\mathrm{dry}} \approx 9.964$, as described in (75), is a very good approximation to the drying time computed from the similarity solution. Figure 5(a) shows a comparison of the drying front $R_{\mathrm{SS}}(t)$ with drying fronts determined previously via asymptotic methods, namely, $R_{\mathrm{Cart}}(t)$ given in (73), and $R_{\mathrm{Sph}}(t)$, given in (79).

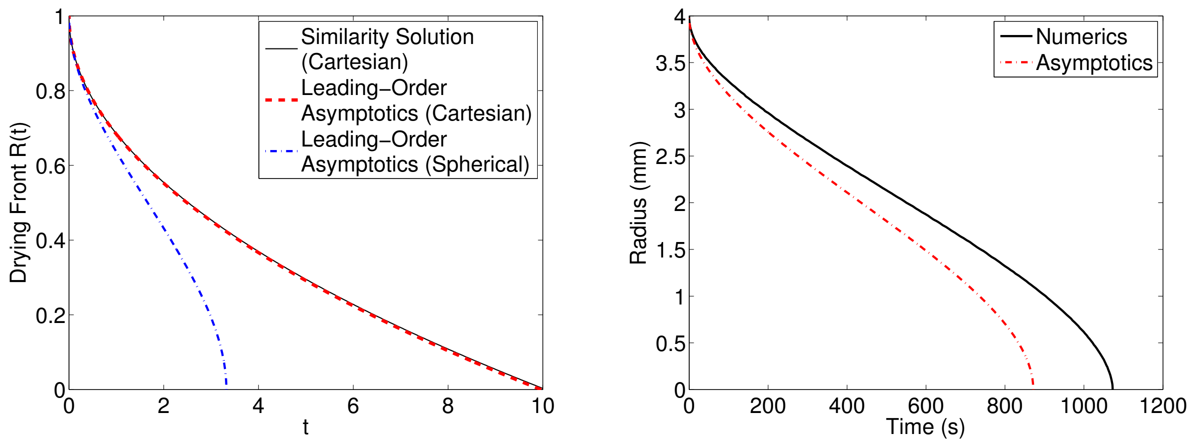

(a) (b)

FIG. 5. *(a) Comparison of the drying fronts $R_{SS}(t)$, $R_{Cart}(t)$, and $R_{Sph}(t)$ in the constant-temperature regime. (b) Comparison of the dimensional drying front $R_{Sph}(t)$, shown in dash-dot red, against the numerical solution of the (dimensional) "simplified" multiphase model from [6] in spherical co-ordinates with $T \equiv 1$, shown in black.*

3.4. Comparison of Asymptotic Approximations with Numerical Results. Comparing these asymptotic approximations with the numerical solutions of (83)-(84), we can see in Figure 5(b), the general shape of the dimensional drying front $R(t)$ agrees well with the dimensional drying front seen in the numerical solution. Because we no longer have the difference between the approximation $T^* \equiv 1$ and the initial condition $T^*(t^*) = T_a < 1$ as we did in Section 2, it is expected that the drying front $R(t)$ determined via asymptotics has a better fit to the numerics. We see, like in Section 2, that the drying time in the numerical solution is larger than $t^{\text{dry}}_{\text{Sph}}$, which was determined from asymptotic results shown in (82). However, this is to be expected; a large (but finite) Stefan number would cause the drying time to be longer than the time produced by the limit $\delta \to 0^+$.

4. Asymptotics of the Multiphase Model for more general evaporation rates with Constant Temperature. In the constant temperature approximation, we have assumed that the evaporation rate I_v has taken the form $I_v(S,P) = (1-P)S(1-\sigma S)$. It is quite possible that this Langmuir's evaporation rate [20] may not be the best way to model water evaporation in a roasting coffee bean. We therefore briefly examine a larger class of evaporation rates in order to highlight the differences a revised model would present. We will now consider a general class of evaporation rates, in which I_v can be written as

$$I_v(S,P) = -\epsilon F(S) G\left(\frac{P-1}{\epsilon}\right), \tag{106}$$

such that F, G are continuous functions independent of ϵ and satisfy the conditions

$$F(0) = 0, \tag{107}$$
$$F(S) > 0 \quad \text{for all} \quad S \in (0,1), \tag{108}$$
$$G(0) = 0, \tag{109}$$
$$G'(0) = \lambda > 0. \tag{110}$$

Physically speaking, (107) implies that evaporation does not occur with zero water content, and (108) indicates that evaporation will not stop if a bean is partially saturated. Additionally, (109) tells us that no evaporation occurs when the vapour pressure is at steam table pressure. However, (110) means that a small decrease in vapour pressure from the steam table pressure will cause evaporation (rather than condensation) to occur. To relate back to Langmuir's evaporation rate, this would be the case where $F(S) = S(1-\sigma S)$ and $G(\psi) = \psi$. Using this general form, the leading-order solutions in Regions i and ii remain the same, as Region i still follows from (109) and Region ii follows from (107). However, in the transition layer, we can show the dynamics for more general classes of evaporation rates. Using the same asymptotic series expansion as shown in Section 2.2, with the additional simplifications of $T \equiv 1$ and $T_1 \equiv 0$, our leading-order solution for (83) becomes

$$-R'(t)\frac{\partial S_0}{\partial \hat{r}} = F(S_0)G(P_1), \tag{111}$$

and our leading-order solution for (84) becomes

$$\delta\left[\frac{\partial^2 P_1}{\partial \hat{r}^2} - \sigma R'(t)\frac{\partial S_0}{\partial \hat{r}}\right] = F(S_0)G(P_1). \tag{112}$$

By equating these two expressions, we determine that, since the matching conditions (32)-(34) remain the same, (89) must also continue to hold:

$$\frac{\partial P_1}{\partial \hat{r}} = R'(t)\left(\frac{1}{\delta} - \sigma\right)(1 - S_0). \tag{113}$$

Thus, the Stefan condition (113) for Region ii is the same, implying that the asymptotics for Regions i and ii are identical for all general evaporation rates of the form stated previously. Now, by dividing (113) by (111), we obtain the following ODE for P_1 in terms of S_0:

$$\frac{dP_1}{dS_0} = -\frac{R'(t)^2\left(\frac{1}{\delta} - \sigma\right)(1 - S_0)}{F(S_0)G(P_1)}. \tag{114}$$

By separating variables, we can integrate (114) and impose the matching conditions (32) once again and obtain

$$\int_0^{P_1} G(\psi)d\psi = (R'(t))^2\left(\frac{1}{\delta} - \sigma\right)\int_0^{1-S_0}\frac{\chi}{F(1-\chi)}d\chi. \tag{115}$$

By defining

$$\mathscr{F}(X) = \int_0^X \frac{\chi}{F(1-\chi)}d\chi, \tag{116}$$

we have that

$$S_0 = 1 - \mathscr{F}^{-1}\left(\frac{\int_0^{P_1} G(\psi)d\psi}{(R'(t))^2\left(\frac{1}{\delta} - \sigma\right)}\right). \tag{117}$$

Substituting (117) into (113), and noting that the function $\mathscr{F}^{-1}$ is only a function of the variable P_1, we can separate the subsequent ODE and obtain that

$$\mathscr{G}(P_1) := \int^{P_1}\frac{d\tilde{P}}{\mathscr{F}^{-1}\left(\frac{\int_0^{\tilde{P}} G(\psi)d\psi}{(R'(t))^2\left(\frac{1}{\delta}-\sigma\right)}\right)} = R'(t)\left(\frac{1}{\delta} - \sigma\right)(\hat{r} - C), \tag{118}$$

where C is chosen so that the matching condition (32) is satisfied. Thus, by a final inversion of the function $\mathscr{G}$, as well as substituting back into (117), our solutions in the transition layer are

$$P_1(\hat{r}, t) = \mathscr{G}^{-1}\left(R'(t)\left(\frac{1}{\delta} - \sigma\right)(\hat{r} - C)\right), \quad S_0(\hat{r}, t) = 1 - \mathscr{F}^{-1}\left(\frac{\int_0^{P_1(\hat{r})} G(\psi)d\psi}{(R'(t))^2\left(\frac{1}{\delta} - \sigma\right)}\right). \tag{119}$$

In general, the functions $\mathscr{F}$, $\mathscr{F}^{-1}$, $\mathscr{G}$, and $\mathscr{G}^{-1}$ are not easy to determine. However, the main purpose of examining the transition layer is to examine the leading-order behaviour of S. One way to do this is to determine the leading-order ODE for S by approximating $G(\psi)$ near $\psi = 0$. Since $P \sim 1 + \epsilon P_1$ in the transition layer, we can make the approximation that $G(P_1) \sim \lambda P_1$. Rearranging (111) and differentiating the expression with respect to $\hat{r}$, as well as substitute in (113), this gives us the ODE

$$\frac{\partial^2 S_0}{\partial \hat{r}^2} - \left(\frac{\partial S_0}{\partial \hat{r}}\right)^2 \frac{F'(S_0)}{F(S_0)} + \lambda\left(\frac{1}{\delta} - \sigma\right)(1 - S_0)F(S_0) = 0. \tag{120}$$

If we allow $u = S_0$ and $w = \left(\frac{\partial S_0}{\partial \hat{r}}\right)^2$, we obtain, in similar nature by methods shown in Section 2.2, that

$$\frac{dw}{du} - 2w\frac{F'(u)}{F(u)} = -2\lambda\left(\frac{1}{\delta} - \sigma\right)(1 - u)F(u). \tag{121}$$

Multiplying (121) by the integrating factor $[F(u)]^{-2}$ as well as ensuring that $w = 0$ when $u = 1$, gives us

$$w = 2\lambda\left(\frac{1}{\delta} - \sigma\right)F(u)^2\int_u^1 \frac{1-\chi}{F(\chi)}d\chi. \tag{122}$$

Thus, if we return to our original variables of the ODE, and choose the negative branch of the square root so $S_0(\hat{r})$ transitions from 1 to 0 as $\hat{r}$ increases, we have

$$\frac{\partial S_0}{\partial \hat{r}} = -F(S_0)\sqrt{2\lambda\left(\frac{1}{\delta} - \sigma\right)\int_{S_0}^1 \frac{1-\chi}{F(\chi)}d\chi}. \tag{123}$$

Motivated by the form of this ODE, we now consider a different evaporation rate that yields an explicit solution for both (119) and (123). Suppose that $F(S) = S^2(1-S)$ and $G(\psi) = \psi$, i.e. $I_v = S^2(1-S)(1-P)$. This implies, after integrating inside the square root, that (123) becomes

$$\frac{\partial S_0}{\partial \hat{r}} = -\sqrt{2\left(\frac{1}{\delta} - \sigma\right)}\left[S_0(1 - S_0)\right]^{\frac{3}{2}}. \tag{124}$$

This ODE can be explicitly solved by separating variables, and its solution is

$$S_0(\hat{r}) = \frac{1}{2}\left[1 - \frac{\hat{r} - C}{\sqrt{(\hat{r} - C)^2 + \frac{8\delta}{1-\delta\sigma}}}\right], \tag{125}$$

where C is an arbitrary constant. This also tells us, from (113), that

$$P_1(\hat{r}, t) = \frac{\left(\frac{1}{\delta} - \sigma\right)R'(t)}{2}\left[\hat{r} - C + \sqrt{(\hat{r} - C)^2 + \frac{8\delta}{1 - \delta\sigma}}\right]. \tag{126}$$

These results can be verified by using (119) and noting that for this choice of $F(S)$ and $G(\psi)$,

$$\begin{aligned} &\mathscr{F}(X) = \frac{X}{1-X}, \quad \mathscr{F}^{-1}(X) = \frac{X}{1+X}, \\ &\mathscr{G}(X) = X - \frac{2\left(R'(t)\right)^2\left(\frac{1}{\delta} - \sigma\right)}{X}, \quad \mathscr{G}^{-1}(X) = \frac{1}{2}\left[X + \sqrt{X^2 + 8\left(R'(t)\right)^2\left(\frac{1}{\delta} - \sigma\right)}\right]. \end{aligned} \tag{127}$$

Therefore, for more general evaporation rates (106) that satisfying conditions (107)-(110), we have now shown that the asymptotic behaviour in Regions i and ii is the same as in the specific earlier case. Additionally, we have determined a general solution for the moisture content and vapour pressure in the transition layer, defined in terms of inverse functions of integrals. These results allow us to conclude that while Langmuir's evaporation rate may not be the best model to describe the evaporation of water in roasting coffee beans, the differences are only observed in the thin transition layer.

5. Discussion. In this paper, we have extended results of the "simplified" form of the multiphase model presented in [6] via asymptotic methods, in order to better understand the qualitative features of the coffee bean roasting process. Motivated by previous numerical results, we considered the limit $\epsilon \to 0^+$, representing the situation where vapour transport rate by Darcy flow is much smaller than the evaporation rate. The asymptotic analysis showed that the solution could be divided into two main regions and a transition layer. The entire bean was in the first region until a time t^*, where a thin transition layer appears at the surface of the bean. This transition layer then propagated into the bean creating a second main region between it and the surface of the bean. This asymptotic limit is different from what has been studied previous in drying models, since the rigid cellulose structure of the solid coffee bean creates a large build-up of vapour pressure before in order to drive the vapour to the external environment. The analysis shows that a narrow drying front, represented by the transition layer, is crucial to the drying process in this limit.

In the first region, the vapour pressure is in equilibrium with the steam table pressure and the moisture content of the bean remains at its initial value, with heat flow governed by the heat equation. In the thin transition region, the moisture content changes rapidly from its initial value to a small value. Here, evaporation dominates and the temperature and vapour pressure remain spatially uniform. Finally, in the second main region, there is almost no water and therefore no evaporation. The problem in this second region consists of diffusion equations for the heat and vapour flow with coupling through the matching conditions, similar to a Stefan problem, at the transition layer.

Numerical simulations suggest that the externally applied roasting temperature is attained globally fairly quickly; hence, the case where temperature is fixed at roasting temperature was considered. This also allowed the coupled Stefan problem to be reduced to a single Stefan problem, which could then be solved via similarity solutions or large Stefan number asymptotics. The leading order expressions are shown to agree well with the dynamics of the drying front found from numerical simulations, under both spherical and planar geometries.

Motivated from the fact that Langmuir's equation, described in [20], may not be the best representation of water evaporation from a coffee bean a more general class of evaporation rates was also examined. By continuing to assume a constant roasting temperature, it was shown that the explicit form of the evaporation rate only affects the dynamics within the transition layer: in particular, how the moisture content S transitions from its initial moisture to zero.

Despite several simplifications made in obtaining asymptotic solutions in each of the regions of the coffee bean, a reasonable agreement between the asymptotic approximations and the numerical solution of the multiphase model as described in [6] has been obtained. This suggests that the asymptotics found here accurately capture the qualitative behaviour of the coffee bean roasting process, and provide an acceptable compromise between a simpler heat transfer model (such as those presented in [5]) and more complicated multiphase models. The asymptotic results presented in this paper can be extended in order to determine the asymptotic dynamics of related heat and mass transfer models. The complete multiphase model described in [6] incorporates variable porosity, and by using similar methods to those shown here, one might determine the leading-order behaviour of the multiphase model with variable porosity. Similarly, one might use the general asymptotic results for the multiphase model discussed here to guide the development of relevant solid mechanics models, which take into account the structural properties of the coffee bean and allow for variations in coffee quality due to structural deformations which may occur during heating and roasting. Asymptotic results may also guide in the development of more complicated models involving many more chemical reactions, as well as in understanding taste and aromatic properties of the final product.

Appendix A. Derivation of the Multiphase Model. Here, we will derive the multiphase model discussed in this paper, which is motivated from the model presented in [6]. The "simplified" multiphase model from [6] is

$$\phi \frac{\partial S}{\partial t} = -I_v, \tag{128}$$

$$\phi \frac{\partial}{\partial t}\left(\frac{(1-S)p_v}{1+\mathscr{T}T}\right) = \frac{1}{\alpha_2} I_v + \mathscr{D}_3 \nabla \cdot \left(\frac{p_v \nabla p_v}{1+\mathscr{T}T}\right), \tag{129}$$

$$\alpha_1 \mathscr{C}_1 (1-\phi)\mathscr{T}\frac{\partial T}{\partial t} + \phi \frac{\partial}{\partial t}\left(S(1+\mathscr{T}T)\right) = -\gamma I_v + \mathscr{T}\left(\left(\zeta_1(1-\phi)+\zeta_3\phi\right)\nabla^2 T + (\zeta_2-\zeta_3)\phi\nabla\cdot(S\nabla T)\right). \tag{130}$$

with the boundary conditions at the surface of the bean

$$\nabla T \cdot \mathbf{n} = (1-T)\frac{\mathrm{Nu}_v \zeta_3 \phi(1-S)}{\zeta_1(1-\phi)+\zeta_2\phi S+\zeta_3\phi(1-S)}, \quad p_v = 1+\mathscr{T} \ \text{ at } \ r=1, \tag{131}$$

the symmetry conditions at the centre of the bean

$$\nabla T \cdot \mathbf{n} = 0, \quad \nabla P \cdot \mathbf{n} = 0 \ \text{ at } \ r=0, \tag{132}$$

the initial conditions

$$S(r,0) = S_0, \quad T(r,0) = 0, \quad P(r,0) = p_{ST}(0), \tag{133}$$

along with

$$I_v = \phi^2 \frac{(p_{ST}-p_v)S(1-S)}{\sqrt{1+\mathscr{T}T}} \ \text{ and } \ p_{ST}(T) = B_1 \exp\left(\frac{B_2\mathscr{T}T}{1+\mathscr{T}T}\right). \tag{134}$$

Here, ϕ is the porosity (the ratio of the total volume the gas and liquid phases occupy to the total representative volume), S is the saturation (the volume fraction of water divided by the total volume of water and gas), I_v is the evaporation rate of water, p_v is the partial pressure of water vapour, T is the normalized temperature, p_{ST} is the steam table pressure, $\mathscr{T} = (T_\infty - T_0)/T_0$, while $\mathscr{D}_3$, α_1, α_2, γ, ζ_1, ζ_2, ζ_3 are dimensionless groups involving physical parameters. We note that in [6], the initial saturation value was defined as S_0. Since this will mean something different in the analysis of this paper, we have changed the initial saturation to be $S_0 \equiv \sigma$. Using the scaling

$$S = \sigma\hat{S}, \quad T = \hat{T}, \quad p_v = p_{ST}(1)\hat{P}, \quad t = \frac{\phi}{\mathscr{D}_3 p_{ST}(1)}\hat{t}, \tag{135}$$

and defining the parameters

$$\epsilon = \frac{\sqrt{\mathscr{D}_3\sqrt{1+\mathscr{T}}}}{\phi}, \quad \delta = \frac{p_{ST}(1)\alpha_2}{\sigma(1+\mathscr{T})}, \quad \beta = \frac{B_2\mathscr{T}}{1+\mathscr{T}}, \tag{136}$$

$$\mathcal{A}_1 = \frac{\sigma\phi}{\alpha_1\mathscr{C}_1(1-\phi)\mathscr{T}}, \quad \mathcal{A}_2 = \gamma\mathcal{A}_1, \quad \mathcal{A}_3 = \frac{\phi(\zeta_1(1-\phi)+\zeta_3\phi)}{\mathscr{D}_3 p_{ST}(1)\alpha_1\mathscr{C}_1(1-\phi)}, \quad \mathcal{A}_4 = \frac{\phi\sigma(\zeta_2-\zeta_3)}{\zeta_1(1-\phi)+\zeta_3\phi}, \tag{137}$$

the model of [6] is put into the form (dropping hats)

$$\frac{\partial S}{\partial t} = -\frac{1}{\epsilon^2}I_v, \tag{138}$$

$$\frac{\partial}{\partial t}\left[\frac{(1+\mathscr{T})P(1-\sigma S)}{1+\mathscr{T}T}\right] = -\frac{1}{\delta}\frac{\partial S}{\partial t} + \nabla\cdot\left[\frac{(1+\mathscr{T})P\nabla P}{1+\mathscr{T}T}\right], \tag{139}$$

$$\frac{\partial T}{\partial t} + \mathcal{A}_1\frac{\partial}{\partial t}\left[S(1+\mathscr{T}T)\right] = \mathcal{A}_2\frac{\partial S}{\partial t} + \mathcal{A}_3\nabla\cdot\left[(1+\mathcal{A}_4 S)\nabla T\right]. \tag{140}$$

Here, the rescaled evaporation rate I_v and the rescaled steam table pressure $P_{ST}(T)$ are given by

$$I_v = S(1-\sigma S)(P_{ST}-P)\sqrt{\frac{1+\mathscr{T}}{1+\mathscr{T}T}} \ \text{ and } \ P_{ST}(T) = \exp\left(\frac{\beta(T-1)}{1+\mathscr{T}T}\right). \tag{141}$$

The boundary conditions we impose on the PDE system (1)-(3) are the symmetry conditions at the centre of the bean

$$\nabla T \cdot \mathbf{n} = 0, \quad \nabla P \cdot \mathbf{n} = 0 \ \text{ at } \ r=0, \tag{142}$$

as well as the heat transfer condition

$$\nabla T \cdot \mathbf{n} = \nu\left(\frac{1-\sigma S}{1-\sigma}\right)\left(\frac{1+\mathcal{A}_4}{1+\mathcal{A}_4 S}\right)(1-T) \ \text{ at } \ r=1, \tag{143}$$

where

$$\nu = \frac{\mathrm{Nu}_v \zeta_3 \phi (1-\sigma)}{(\zeta_1(1-\phi)+\zeta_3\phi)(1+\mathcal{A}_4)}. \tag{144}$$

Previously, the model introduced in [6] imposes a Dirichlet condition in P at the surface of the bean. We will instead impose a different boundary condition for P in order to prevent condensation from occurring at the surface of the bean. This can be achieved by imposing that P is aligned with the steam table pressure for temperatures below the evaporating temperature, i.e.

$$P\big|_{r=1} = \begin{cases} P_{ST}(T), & T < T_a, \\ P_a, & T \geq T_a. \end{cases} \tag{145}$$

Here, $P_a := \frac{1+\mathscr{T}}{p_{ST}(1)}$ and $T_a := P_{ST}^{-1}(P_a)$. We will also make the assumption that the change in boundary conditions for P only occurs at one critical time, namely, t^*. We define t^* as when the time when the evaporation temperature T_a is achieved at the surface of the bean, i.e. as the solution to the equation $T(1,t^*) = T_a$. Finally, we impose the initial conditions corresponding to uniform initial moisture content, room temperature, and equilibrium steam table pressure, i.e.

$$S(r,0) = 1, \quad T(r,0) = 0, \quad P(r,0) = P_{ST}(0). \tag{146}$$

REFERENCES

[1] J.M. Talbot, Grounds for agreement: The political economy of the coffee commodity chain. Rowman and Littlefield, Oxford, UK (2004).

[2] J. Baggenstoss, Coffee roasting and quenching technology - Formation and stability of aroma compounds. PhD thesis, Swiss Federal Institute of Technology (2008).

[3] S. Schenker, Investigations on the hot air roasting of coffee. PhD thesis, Swiss Federal Institute of Technology, Zurich (2000).

[4] X. Wang and L.T. Lim, *A kinetics and modeling study of coffee roasting under isothermal conditions*, Food and Bioprocess Technology, 7 (2014), pp. 621-632.

[5] A. Fabbri, C. Cevoli, L. Alessandrini, and S. Romani, *Numerical modeling of heat and mass transfer during coffee roasting process*, Journal of Food Engineering, 105 (2011), pp. 264-269.

[6] N.T. Fadai, J. Melrose, C.P. Please, A. Schulman, R.A. Van Gorder, *A Heat and Mass Transfer Study of Coffee Bean Roasting*, preprint (2016).

[7] K.M. Moroney, W.T. Lee, S.B.G. O'Brien, F. Suijver, J. Marra, *Modelling of coffee extraction during brewing using multiscale methods: an experimentally validated model*, Chemical Engineering Science, 137 (2015), pp. 216-234.

[8] W.N. Hernandez-Diaz, I.I. Ruiz-Lopez, M.A. Salgado-Cervantes, G.C. Rodriguez-Jimenez, and M.A. Garcia-Alvarado, *Modeling heat and mass transfer during drying of green coffee beans using prolate spheroidal geometry*, Journal of Food Engineering, 86 (2008), pp. 1-9.

[9] A. Halder, A. Dhall, and A.K. Datta, *Modeling transport in porous media with phase change: applications to food processing*, Journal of Heat Transfer, 133 (2011), 031010.

[10] H. Ni and A.K. Datta, *Heat and moisture transfer in baking of potato slabs*, Drying Technology 17 (1999), pp. 2069-2092.

[11] A. Dhall, A. Halder, and A.K. Datta, *Multiphase and multicomponent transport with phase change during meat cooking*, Journal of Food Engineering, 113 (2012), pp. 299-309.

[12] Y. Llave, K. Takemori, M. Fukuoka, T. Takemori, H. Tomita, and N. Sakai, *Mathematical modeling of shrinkage deformation in eggplant undergoing simultaneous heat and mass transfer during convection-oven roasting*, Journal of Food Engineering, 178 (2016), pp. 124-136.

[13] H. Huang, P. Lin, and W. Zhou, *Moisture transport and diffusive instability during bread baking*, SIAM Journal on Applied Mathematics, 68 (2007), pp. 222-238.

[14] J Chen, K Pitchai, S Birla, M Negahban, D Jones, J Subbiah, *Heat and Mass Transport during Microwave Heating of Mashed Potato in Domestic Oven-Model Development, Validation, and Sensitivity Analysis*, Journal of Food Science 79, pp. E1991-E2004.

[15] J. Zhang and A.K. Datta, *Mathematical modeling of bread baking process*, Journal of Food Engineering, 75 (2006), pp. 78-89.

[16] M. A. Stanish, G. S. Schajer, and F. Kayihan, *A Mathematical Model of Drying for Hygroscopic Porous Media*, AIChE Journal, 32 (1986), pp. 1301-1311.

[17] S. K. Truscott and I. W. Turner, *A heterogeneous three-dimensional computational model for wood drying*, Applied Mathematical Modelling, 29 (2005), pp. 381-410.

[18] P. Chen and D. C. T. Pei, *A Mathematical Model of Drying Processes*, International Journal of Heat and Mass Transfer, 32 (1989), pp. 297-310.

[19] A. M. Meirmanov, The Stefan Problem, De Gruyter Expositions in Mathematics, Berlin: De Gruyter (1992).

[20] I. Langmuir, *The Vapor Pressure of Metallic Tungsten*, Physical Review, 2 (1913), pp. 329-342.